

# Different ocular dominance map formation by influence of orientation columns

M. W. Cho & S. Kim

Department of Physics, Pohang University of Science and Technology, Kyungpook, Pohang, 790-784, South Korea

In the mammalian visual cortex, the observed ocular dominance (OD) patterns are distinguished as at least three different types. In macaque monkeys, the OD columns form parallel bands of regular spacing with relatively few branching points and mainly oriented perpendicular to area boundaries<sup>1</sup>. The degree of OD segregation is strong and the average typical spacing  $\Lambda_{OD}$  is larger than that of orientation preference (OP) columns ( $\Lambda_{OD} > \Lambda_{OP}$ )<sup>2</sup>. In cats, the OD columns form an array of beaded bands exhibiting only a small tendency of elongation orthogonal to area boundaries<sup>3,4</sup>. The degree of OD segregation is intermediate and  $\Lambda_{OD}$  is smaller than that of OP columns ( $\Lambda_{OD} < \Lambda_{OP}$ )<sup>5</sup>. In the case of tree shrews, the OD segregation is very weak or absent. There exhibit more stripe-like patterns in extensive OP column regions and consequently low densities of orientation centres, so-called pinwheels, observed<sup>26</sup>. Here we will show that such different OD pattern formation types and OD segregation strength are origin to anisotropy  $\lambda$ , which will be defined as the ratio of the interaction strength between OD and OP columns. The anisotropy  $\lambda$  is very significant value to not only determine the OD map formation type but also influence on the OP pattern regularity or the pinwheel annihilation rate. We will show that the existence of the thresholds among different OD pattern formation types depending on the anisotropy and compare it with the anisotropy of each species from experimental data. Finally, we will discuss a larger spacing of OD columns in squinters compared to normal animals.

It is well-known property that OP and OD patterns are not independent, but are correlated. OP and OD slabs are each aligned with an individual common axis, and these axes are orthogonal (“global orthogonality”). Pinwheels tend to align with the centers of OD bands and iso-orientation contours intersect borders of OD bands at right or steep angles (“local orthogonality”)<sup>2</sup>. We infer the correlation between the OP and OD columns is due to the normalization of synapse strength. The orthogonality between the iso-orientation contours and the borders of opposite ocular dominance can be derived from the equilibrium and normalization condition with model independently (see Methods). This constraint is neurobiologically origin to the homeostatis or synapse plasticity rule, that the sum of all the synaptic weights (or of their square values) of synapses impinging on the cell remains constant or a conserved sum of the synaptic weights of all contacts made in the network by the same parent axon<sup>6</sup>. When response properties of cortical cells or small cortical regions at each cortical location  $\mathbf{r}$  are represented by a usual feature vector<sup>7</sup>,

$$\Phi(\mathbf{r}) = (|q(\mathbf{r})| \cos 2\phi(\mathbf{r}), |q(\mathbf{r})| \sin 2\phi(\mathbf{r}), z(\mathbf{r})) \quad (1)$$

for preferred orientations  $\phi(\mathbf{r})$ , and the ocular dominance  $z(\mathbf{r})$ , the imposed restriction for normalization is  $|q(\mathbf{r})|^2/|q_{max}|^2 + |z(\mathbf{r})|^2/|z_{max}|^2 = 1$  for all  $\mathbf{r}$ .  $|q(\mathbf{r})|$ , which measures the orientation selectivity of the average response of neurons, vanishes at pinwheel centres so that strong ocular dominance can occur near pinwheel centres from the normalization constraint. Similar phenomena is known in distinct but familiar systems, that there are also the development of strong strength at scalar components

near the singularity centres at orientational components with the normalization constraint. (In-plane) vortex, the leading actor for the ability of superconductors and superfluids, are equivalent structures with the pinwheels as singularity at the orientational components. The formation of island structure at the scalar components near the singular centres is known as the development of out-of-plane vortex in magnetism.

The conventional spin vector  $\mathbf{S}_i = (S_i^x, S_i^y, S_i^z)$  resemble equation (1) and become another useful representation of feature vector with the preferred orientation  $\phi_i = (1/2) \tan^{-1}(S_i^y/S_i^x)$  and the ocular dominance  $S_i^z$ . We build a visual map formation method by non-competitive and lateral interactions rule, described by the spin-like Hamiltonian,

$$H = - \sum_{i,j} \{ J_{OP}(\mathbf{r}_{ij})(S_i^x S_j^x + S_i^y S_j^y) + J_{OD}(\mathbf{r}_{ij})S_i^z S_j^z \}, \quad (2)$$

where  $J_\mu(\mathbf{r}) = (\varepsilon_\mu/2)I_\mu(\mathbf{r})$  ( $\mu = OP$  or  $OD$ ) is a interaction strength with Mexican hat type in OP or OD column. Every components are normalized by unit ( $|\mathbf{S}_i|^2 = 1$ ) and the maximal activity rate  $|q_{max}|$  and  $|z_{max}|$  are embraced in  $\varepsilon_{OP}$  and  $\varepsilon_{OD}$ , means the learning rate due to the Hebbian rule. We consider the Mexican hat type function  $I_\mu(\mathbf{r})$  is described by at least two parameters, the inhibitory strength  $k_\mu$  and the cooperation range  $\sigma_\mu$ . We use the lateral neighborhood interaction function  $I$ , modified from a wavelet, as

$$I_\mu(\mathbf{r}) = \left( 1 - k_\mu \frac{r^2}{\sigma_\mu^2} \right) \exp(-r^2/2\sigma_\mu^2). \quad (3)$$

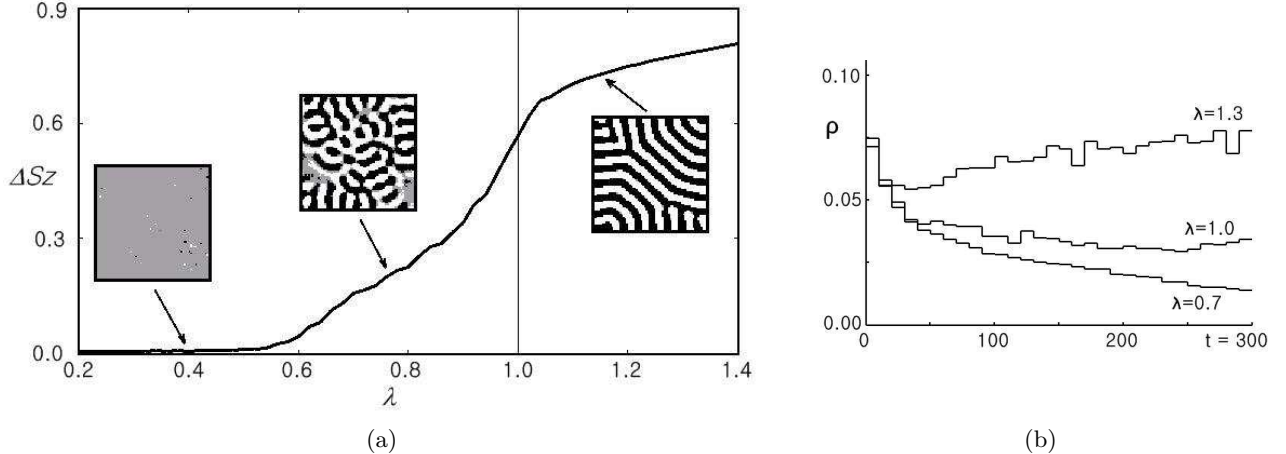


**Figure 1:** (a) Simulation results of the OD segregation strength and the different OD pattern formation depending on anisotropy  $\lambda$ . Segregation strength are measured by the standard deviation  $\Delta S_z$  and the segregation absent regions ( $|S_z| \leq 0.01$ ) are presented by gray color. Simulation conditions are  $\sigma_{OP}^2 = \sigma_{OD}^2 = 6.$ ,  $k_{OP} = k_{OD} = 1.0$  ( $\lambda = \varepsilon_{OD}/\varepsilon_{OP}$ ) and the typical spacing of OD pattern is  $\Lambda_{OD} \simeq 8.9$ . Maps are generated by metropolis algorithm at zero temperature, with non-periodic boundary condition and an initially random state in  $70 \times 70$  lattice.  $\Delta S_z$  are measured at given time  $t = 100$  and averaged after 10 times evolutions for given  $\lambda$ . (b) The pinwheel density  $\rho(t)$  as a function of development time with the anisotropy  $\lambda = 0.7, 1.0$  and  $1.3$ .

It is not matter to use another Mexican hat type function such as the difference of Gaussians (DOG) filters,  $I_{DOG}(\mathbf{r}) = \exp(-r^2/2\sigma_1^2) - k \exp(-r^2/2\sigma_2^2)$ .

The study of vortex behaviour in magnetism offer useful results in our issue. The classical two-dimensional anisotropic Heisenberg model (CTDAHM), applied for superfluid films or superconductors, is described by the Hamiltonian,

$$H = - \sum_{\langle i,j \rangle} K (S_i^x S_j^x + S_i^y S_j^y + \lambda S_i^z S_j^z), \quad (4)$$

where  $K > 0$  is the exchange coupling constant and  $\langle i,j \rangle$  are to be understood as first neighborhood indices in a lattice. The parameter  $\lambda$  describes the anisotropy between two different components, called in-plane and out-of-plane in magnetism. It is obtained the so-called pure Heisenberg model for  $\lambda = 1$ , the boundary of two different solutions. For  $\lambda < 1$  (or  $\lambda > 1$ ), the same thermodynamic behaviour is expected since the system is in the same universality class as the XY (or Ising) model. Thermodynamic properties of (4) are well understood in the limit  $\lambda = 0$  following the work of Berezinskii<sup>8</sup> and Kosterlitz and Thouless<sup>9</sup>. It has a phase transition at temperature  $T_{KT}$ , named Kosterlitz-Thouless phase transition, which is characterized by a vortex-antivortex unbinding or the stability of isolated vortices. The possibility of two types of vortex solutions (in-plane and out-of-plane) in the two-dimensional anisotropic Heisenberg model was first discussed by Takeno and Homma<sup>10</sup> and different values of the critical anisotropy  $\lambda_c$ , above which out-of-plane vortices are stabilized, were found depending on the lattice type ( $\lambda_c \approx 0.72, 0.82, 0.62$  for square, honeycomb, and triangular lattices, respectively) by Gouv  a *et*

*al.* 11

Comparing with (4), the anisotropy  $\lambda$  in (2) will be the ratio of interaction strength in OP and OD columns,  $\lambda \sim J_{OD}/J_{OP}$  or  $\lambda \propto \varepsilon_{OD}/\varepsilon_{OP} \simeq |z_{max}|/|q_{max}|$ . The co-operation ranges  $\sigma_\mu$  also exert influence on the anisotropy parameter. The interaction strength in  $d$ -dimension is in proportion to  $\sigma_\mu^d$ , which is the number of interacting pairs ( $\lambda \propto \sigma_{OD}^2/\sigma_{OP}^2$ ). The anisotropy can occur by different strength of lateral inhibitory  $k_\mu$ . In the study of numerical simulations by equation (2), we can find the emergence of three different OD pattern types, where parallel bands patterns with strong OD segregation for  $\lambda > 1$ , beaded bands patterns with intermediate segregation for  $\lambda_c < \lambda < 1$ , and OD segregation absent in whole region for  $\lambda < \lambda_c$ , which corresponds with observed pattern in the OD columns of macaque monkey, cat and tree shrew, respectively (Fig. 1.(a)). We measure the degree of OD segregation as the standard deviation of the normalized ocular dominance,  $\Delta S_z$  ( $0 \leq \Delta S_z \leq 1$ ) at zero temperature and find that the OD segregation strength also increases according to the anisotropy  $\lambda$ . Three different behaviours of OD pattern formation depending on the anisotropy are evidently related with the crossover behaviour of the solutions in the CTDAHM.

Pinwheel annihilation during visual map development is related to the thermodynamic behaviours of in-plane vortices below  $T_{KT}$ . The variation of  $T_{KT}$  with  $\lambda$  is important in magnetism also. Hikami and Tsuneto<sup>12</sup> derived that  $T_{KT}$  decreases monotonously to 0 as  $\lambda$  increases and approaches to 1. This results can be translated into our issue like that the pinwheel structures last longer or even become stabilized with small thermal fluctuations in the presence of the strong activity in OD

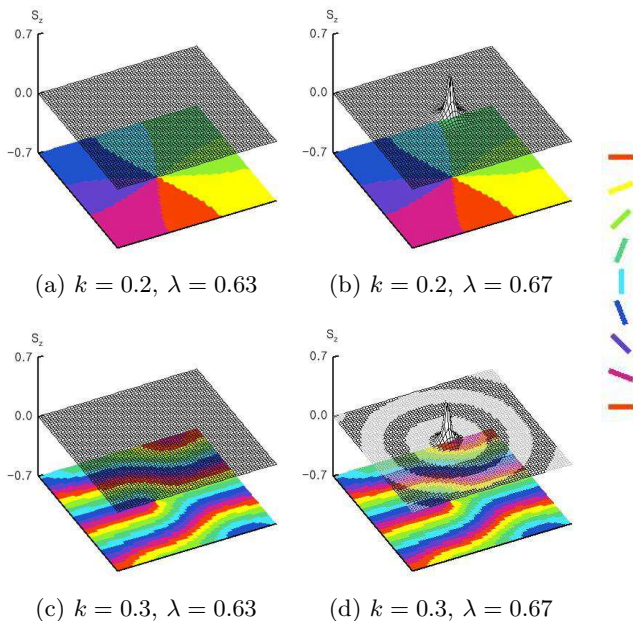


**Figure 2:** The singularity in OP column and the development of peak in OD column. They are started from initially prespecified state with  $\sigma_{OD}^2 = \sigma_{OP}^2 = 6$ ,  $k_{OD} = k_{OP}$  (so  $\lambda = \varepsilon_{OD}/\varepsilon_{OP}$ ),  $60 \times 60$  lattice size and non-periodic boundary condition. OP maps are presented by 8 different color according to the prefer angle  $\phi(\mathbf{r})$ . OD columns ( $S_z$  components) are presented by frame lines with black color for  $S_z(\mathbf{r}) \geq 0$  or gray color for otherwises. A singular point exists with radial extension of the iso-orientation contours  $k < k_c$  ( $= 1/4$ ) or with plane-waves for  $k > k_c$ . There exist the threshold  $\lambda_c$ , below which the development of ocular dominance is absent (b & c). Above  $\lambda_c$ , a peak emerges in OD column near the singular point and the peak decreases monotonously from the centre for  $k < k_c$  or with pulse-shape for  $k > k_c$ .

columns. Wolf and Geisel first noted that the presence of ocular dominance columns impedes pinwheel annihilation from analytic and simulational results<sup>13</sup>. Fig. 1(b) shows the variations of pinwheel densities as a function of development time (x-axis) during development for different anisotropy. Wolf and Geisel showed similar simulational results with elastic net model for different degree of OD segregation rather than anisotropy.

In contrast to the CTDAHM in (4), the spin Hamiltonian for visual map formation in (2) has inhomogeneous solutions, which make the emergence of the linear zones in OP maps and the parallel bands in OD maps, if the lateral inhibitory strength  $k$  is larger than a threshold ( $k_c = 1/4$ ). The single vortex simulations in Fig. 2 show the structure of two different vortex types and the development of out-of-plane vortices (beaded OD pattern) near the centre of in-plane vortices (or pinwheels) depending on anisotropy parameter  $\lambda$ . For  $k < k_c$ , the peak near the orientational singularity in Fig. 2b is a typical feature of in-plane and out-of-plane vortices observed in magnetism. For  $k > k_c$ , vortices exist with periodic so-

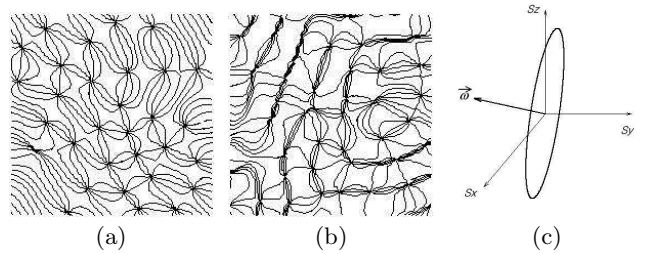


**Figure 3:** (a) The iso-orientation contours of simulation results for  $\lambda = 0.83$  and (b)  $\lambda = 1.38$ . The iso-orientation contours for  $\lambda > 1$  show non-regular distribution comparing with those for  $\lambda < 1$ . It is because the angular velocity vector of phase space  $\hat{\omega}$  too slant like (c) and the trajectories in  $Sx - Sy$  plane are shrunken to ellipse or line. ( $\lambda = \varepsilon_{OD}/\varepsilon_{OP}$ ,  $\sigma_{OP}^2 = \sigma_{OD}^2 = 10$ ,  $k_{OD} = k_{OP} = 0.5$  and  $50 \times 50$  lattice size)

lutions, which make the linear zones in OP or the band structures in OD column. The emergence of the beaded band pattern in the OD columns of cat are related with the development of the pulse-shaped out-of-plane components near the singularity in Fig. 2d.

For  $\lambda > 1$ , the influences of OD column become stronger than that of orientation column and lead the whole map formation. Parallel bands appear in whole range of OD columns and make right or steep angle with area boundaries, which are the typical properties of OD patterns generated without OP columns. The columnar OP pattern exist yet, but are less regular. The distribution of iso-orientation contours is not even and locally too dense or sparse (Fig.3). The angular velocity vector  $\hat{\omega}(\mathbf{r})$  defined in the feature vector space help to understand this. For  $\lambda = 1$ , map formation progress is balanced between two universal solutions as the XY or the Ising model. The angular velocity vectors of phase space  $\hat{\omega}$  sustain their slant with  $|\hat{\omega}_x| = |\hat{\omega}_y| = |\hat{\omega}_z| = 1/\sqrt{3}$  without falling into  $S_x - S_y$  plane or standing up into  $S_z$  axis and  $\Delta S_z$  is conserved as  $\sqrt{1 - |\hat{\omega}_z|^2}/\sqrt{2} = 1/\sqrt{3} \simeq 0.577$  as shown in Fig. 1 ( $1/\sqrt{2}$  is the standard deviation of sinusoidal function). For  $\lambda > 1$  (or  $\lambda < 1$ ), the rotational plane start to lay vertically (or horizontally) and  $\Delta S_z$  approaches 1 (or 0) in map formation progresses. When the rotational plane are too slant, the trajectory circles in  $Sx - Sy$  plane are shrunken to ellipses or lines and the velocities in  $\phi$  coordinate become irregular.

It can be uncertain which factor among the activity rate  $\varepsilon_\mu$ , the cooperation ranges  $\sigma_\mu$  and the lateral inhibitory strength  $k_\mu$  mainly occurs the anisotropy between OP and OD columns *in vivo*. We can infer it by comparing the typical spacing  $\Lambda_{OP}$  and  $\Lambda_{OD}$  measured in experiments. The typical spacing  $\Lambda_\mu$  is predicted to be proportional to  $\sigma_\mu$  with model independently<sup>14,15,16</sup>. If there is only the difference of the activity rate  $\varepsilon_\mu$  between OP and OD columns, the typical spacing have to be same ( $\Lambda_{OD} = \Lambda_{OP}$  for all  $\lambda$ ). For the difference of  $k_\mu$ , the typical spacing of OD bands will be smaller than that of OP slabs when strong OD segregations ( $\Lambda_{OD} < \Lambda_{OP}$

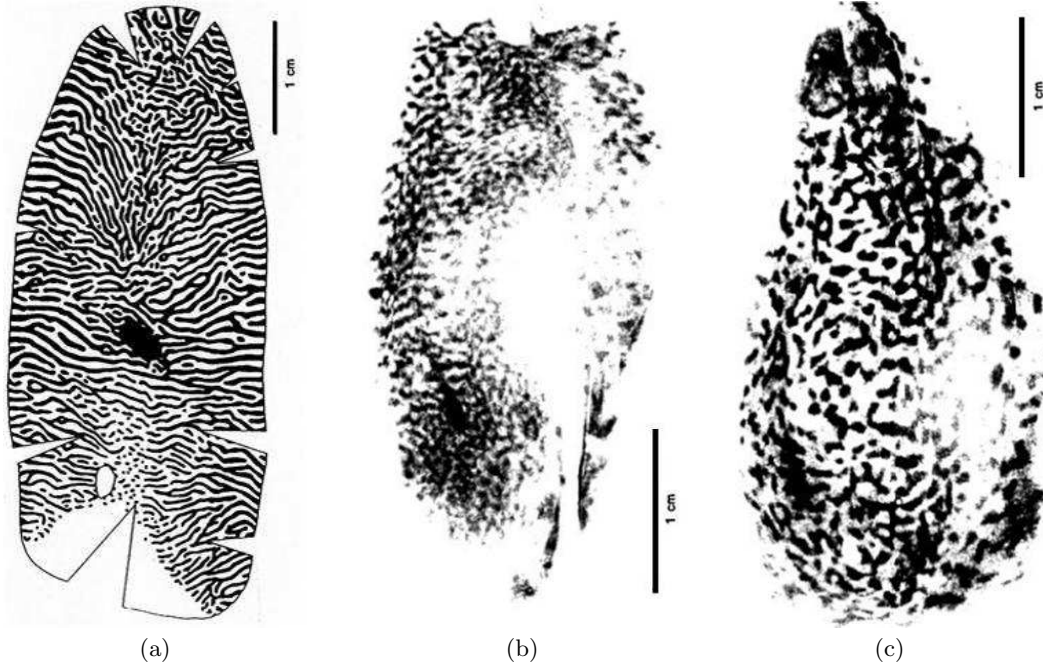


**Figure 4:** Pattern of OD columns in the visual cortex of (a) normally raised macaque monkey (ref. 1) (b) normally raised cat (ref. 17) and (c) a cat raised with artificially induced squint (ref. 17). The OD columns in macaque monkey form parallel bands of regular spacing with relatively few branching points. These bands are mainly oriented perpendicular to area boundaries. The OD columns in both normal and strabismic cat form an array of beaded bands but the periodicity of the OD columns is wider in the strabismic cat (Copyright 1985, 1994 by the Society for Neuroscience).

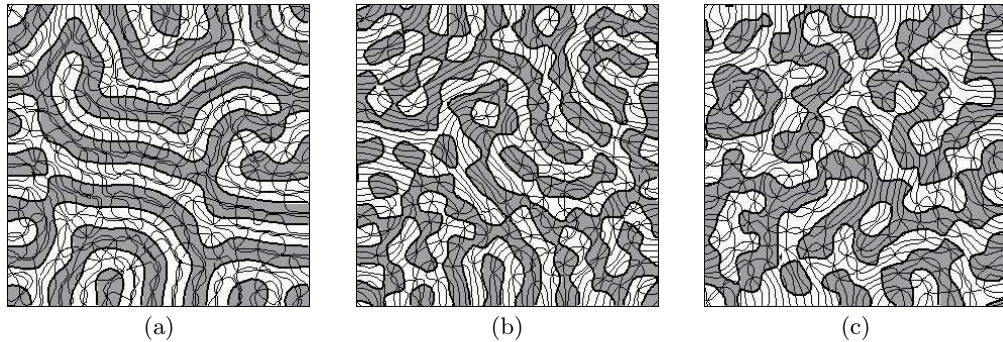


**Figure 5:** Simulations of OD and OP maps with different typical spacing  $\Lambda_{OP}$  and  $\Lambda_{OD}$ . (a) Evolution with larger cooperation range of OP column than that of OD column for normal macaque monkey ( $\sigma_{OD}^2 = 13.8$ ,  $\sigma_{OP}^2 = 10.0$ ,  $k_{OP} = k_{OD} = 0.7$ ,  $\Lambda_{OD} \simeq 11.3$ ,  $\Lambda_{OP} \simeq 14.5$ , and  $\lambda = \sigma_{OD}^2/\sigma_{OP}^2 = \Lambda_{OD}^2/\Lambda_{OP}^2 \simeq 1.38$ ) and (b) evolution with larger cooperation range of OD column than that of OP column for normal cat ( $\sigma_{OD}^2 = 6.7$ ,  $\sigma_{OP}^2 = 10.0$ ,  $k_{OP} = k_{OD} = 0.7$ ,  $\Lambda_{OD} \simeq 10.1$ ,  $\Lambda_{OP} \simeq 12.4$  and  $\lambda \simeq 0.67$ ). The ratio of the cooperation range  $\sigma_\mu$  per each column is according to the experimental data (Table.1). More parallel bands like OD patterns of macaque monkey for  $\lambda > 1$  (or beaded bands like those of cat for  $\lambda < 1$ ) emerge. (c) Evolution with small inhibitory strength of OD columns  $k_{OD}$  for strabismic cat. ( $\sigma_{OD}^2 = 6.7$ ,  $\sigma_{OP}^2 = 10$ ,  $k_{OD} = 0.35$ ,  $k_{OP} = 0.7$ ,  $\Lambda_{OD} \simeq 15.2$ ,  $\Lambda_{OP} \simeq 14.5$  and  $\lambda = (\sigma_{OD}^2/\sigma_{OP}^2)(k_{OD}/k_{OP}) \exp(1/2k_{OD} - 1/2k_{OP}) \simeq 0.68$ ). Other conditions are  $\varepsilon_{OD} = \varepsilon_{OP}$ , 100  $\times$  100 lattice size and non-periodic boundary conditions.

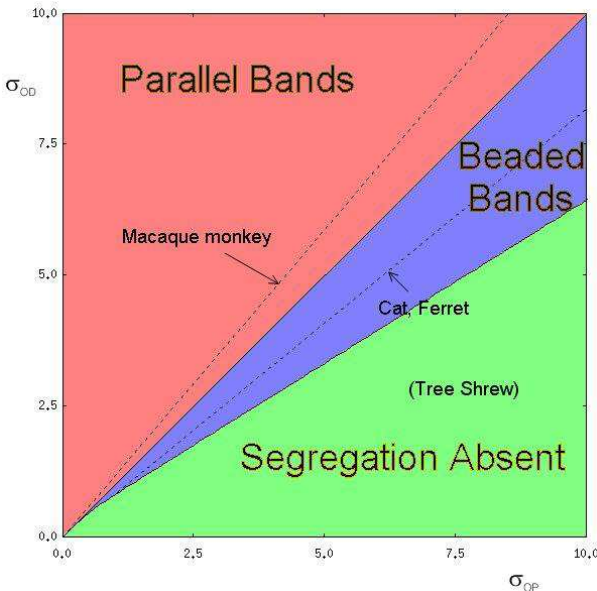
for  $\lambda > 1$ ). But only for the difference of  $\sigma_\mu$ , the typical spacing of OD bands are larger than that of OP slabs when strong OD segregations ( $\Lambda_{OD} > \Lambda_{OP}$  for  $\lambda > 1$ ) like the experimental data in macaque monkey and cat (Table.1). So we can conclude that the reason of the different OD appearance between macaque monkey and cat is because of the different cooperation range  $\sigma$  between

OD and OP columns. We obtain simulation results with different cooperation range  $\sigma_\mu$  between the OP and the OD columns according to the experimental data. More beaded bands in OD columns emerge near the pinwheels like the visual patterns of cat for  $\Lambda_{OD} < \Lambda_{OP}$  (Fig. 5 (a)), whereas parallel bands in OD map emerge in whole range like those of macaque monkey for  $\Lambda_{OD} > \Lambda_{OP}$

**Table 1:** Wavelength of OD and OP columns and OD segregation for different animals

| Species                     | $\Lambda_{OD}$ [mm] | $\Lambda_{OP}$ [mm] | $\Lambda_{OD}^2/\Lambda_{OP}^2$ | $\rho$ [1/mm <sup>2</sup> ] | $\hat{\rho} = \rho\Lambda_{OP}^2$ | OD pattern     | OD segregation |
|-----------------------------|---------------------|---------------------|---------------------------------|-----------------------------|-----------------------------------|----------------|----------------|
| Macaque monkey <sup>a</sup> | 0.80                | 0.68                | 1.38                            | 8.1                         | 3.75                              | parallel bands | strong         |
| Normal cat <sup>b</sup>     | 0.8-1.0             | 1.0-1.2             | ~0.67                           | 2.1-2.4                     | 2.5-2.9                           | beaded bands   | intermediate   |
| Strabismic cat <sup>c</sup> | 1.1-1.3             | 1.0-1.3             | ~1.1                            | 2.7                         | 3.57                              | beaded bands   | intermediate   |
| Ferret <sup>d</sup>         | 0.61                | 0.75                | 0.66                            | 5.5                         | 2.85                              | beaded bands   | intermediate   |
| Tree shrew <sup>e</sup>     |                     | 0.52                |                                 | 2.1-2.6                     |                                   |                | absent         |

<sup>a</sup> Data from ref. 2. <sup>b</sup> Spacing of OD from ref. 3,17, spacing of OP from ref. 5,21,22 and pinwheel density from ref. 23,24. <sup>c</sup> Data from ref. 18. Löwel *et al.* <sup>18</sup> used a different algorithm with Rao *et al.* <sup>23</sup> and Bonhoeffer *et al.* <sup>24</sup> and obtain average density of pinwheel centres in area 17 of normally raised cats as  $2.6 \pm 0.1/\text{mm}^2$ , in the same range as the value observed in strabismic cats. <sup>d</sup> Data of OD from ref. 25 and OP from ref. 23. <sup>e</sup> Data from ref. 26.

**Figure 6:** The phase diagram of ocular dominance pattern according to the cooperation ranges and the experimental data per species.

(Fig. 5 (b)).

The spacing of OD columns in squinting cats is known to be larger than in normally raised animals<sup>17</sup>. In area 17 of strabismic animals, the spacing of adjacent OD columns is about 20-30% larger compared with that in normally raised cats and resembles the spacing of the iso-orientation domains<sup>18</sup>. The actual mechanism by which squint leads to a larger spacing of OD columns is presently unknown. One of noticeable fact is that the OD columns of strabismic cats forms beaded bands however the spacing of OD columns is equal or larger than that of OP columns (Table.1). The difference of activity rate  $\varepsilon_\mu$  or the cooperation range  $\sigma_\mu$  cannot form such visual map pattern type. If  $\sigma_{OD}$  of strabismic cat is larger than that of normal cat, parallel band types will be emergent

in the OD column of strabismic cat. We suggest that the elimination of correlated activity between the two eyes has effect on the lateral suppression in OD column. There are experimental evidence that the development of tangential intracortical connections depends on use-dependent selection mechanisms similar to those in the development of thalamocortical connections<sup>19</sup>. Neurons wire together if they fire together and lateral inhibition concentrates in the neighborhood of each neuron for the correlated activity in normal cat. There are already simulations with lateral connection model showing the variation of OD wavelength depending on the inhibitory strength<sup>20</sup> before we obtain the wavelength by analytic calculation<sup>16</sup>. We can obtain similar visual map formation with strabismic cats in simulations for  $k_{OD} < k_{OP}$  (Fig. 5 (c)).

The critical anisotropy  $\lambda_c$ , above which out-of-plane vortex develop, have various value depending on the interaction function  $J_\mu(\mathbf{r})$  and the lattice types. The exact calculation of the critical anisotropy is important problem in magnetism also<sup>27</sup>. It is said that any continuum theory will fail in calculation of  $\lambda_c$  because of the singularity near vortex core<sup>28</sup>. The critical anisotropies of different lattice types in the classical model with nearest-neighbor interactions is precisely calculated by Wysin<sup>29</sup>. We expand his analytic methods to the distant interaction models and also build a simulational method to obtain the critical anisotropy precisely. We find the critical anisotropy  $\lambda_c$  for different  $J_\mu(\mathbf{r})$  and lattice types in analytic calculations and simulational experiments. We find that the boundary of out-of-plane vortex stability can be described as  $\sigma_{OD} \simeq \alpha \sigma_{OP} + \beta$ . The gradient  $\alpha$  agree relevantly for different lattice types and has small variance depending on the inhibitory strength  $k$ . The intercept  $\beta$  is relatively smaller than  $\alpha$  and the region for the beaded band pattern can be described by  $\alpha < \sigma_{OD}/\sigma_{OP} < 1$  where  $\alpha \sim 0.6$ . It agrees with the experimental data that  $\Lambda_{OD}/\Lambda_{OP}$  in cat and ferret is  $\sim 0.82$ . Fig. 6 shows the phase diagram of OD pattern formation with the cooperation ranges  $\sigma_{OP}$  and  $\sigma_{OD}$ . We will show the detailed

procedure to obtain the critical anisotropy  $\lambda_c$  in physical journal<sup>30</sup>.

However nearly all proposed development model of visual cortical map are based on a common set of postulates<sup>31</sup>, they are focused on different cortical modification rule. There was a comparison between proposed models and the experimental data for the relationships between OP and OD maps<sup>7</sup>. Analytical analysis for different models share some common results that are the proportional relationship between the typical spacing  $\Lambda_\mu$  and the cooperation range  $\sigma_\mu$ , the existence of bifurcation between homogeneous and inhomogeneous state, and the influence of the presence of OD columns on pinwheel annihilation. We demonstrate without model specification that the correlations between two columns occur using the normalization of synapse strength (see Methods). There are another suggestion to explain the different layout of visual cortical patterns between species by the different cooperation range  $\sigma$  between OP and OD columns. Hoffsmüller *et al.* pointed out the bifurcation from homogeneous to inhomogeneous states as the cooperation range  $\sigma$  decrease in competitive Hebbian models and suggested a sequential bifurcation scenario which explains the different pattern types through dynamics rearrangement, bound to the already established other column pattern formation<sup>32,33</sup>. Wolf *et al.* suggested that larger spacing of OD columns in squint is also due to the different developmental order of OP and OD columns<sup>34</sup>. There is no explain yet by the sequential bifurcation scenario for the segregation absence in OD columns of tree shrew. We show that lateral interaction model has the bifurcation between homogeneous and inhomogeneous state depending on the inhibitory strength  $k$  in lateral interactions rather than the cooperation range  $\sigma$  so that cannot follow the sequential bifurcation scenario<sup>16</sup>. We think the difference of interaction strength between OP and OD columns determines the type of OD pattern formation without any more complex scheme, however the anisotropy  $\lambda$  can have various definitions depending on respective models.

We show that the typical behaviours in the visual map formation are belong to a universality class. Pinwheels in OP or beaded bands pattern in OD columns are acquainted structures by different names in distinct systems. We suggested a general method to reduce the complex process of neural interactions at the cortical level<sup>16</sup>. The differential geometric idea says that the major feature of the visual cortical map is not determined by the detailed cortical modification rule but the lattice geometry and the symmetry group in pattern space. We believe that the most cortical map formation problem, in particular of primary sensory area, will be generalized with simple descriptions by this method.

## Methods

However any cortical modification rule is used, the energy function for pattern formation has to obey some invariant constraint. When we perform rotations in all the preferred angles  $\phi$  through same angle  $\chi$  ( $\phi \rightarrow \phi + \chi$  - called ‘global’ gauge transform), the total summation in energy function is invariant and the possible effective Hamiltonian as a function of the preferred angle  $\phi$  is that

$$H[\phi] = \int dr^2 \{a_2(\nabla\phi)^2 + a_4(\nabla\phi)^4 \dots\}. \quad (5)$$

The invariant is broken down if there are  $\phi, \phi^2 \dots \phi^n$  terms. The odd power terms of gradient,  $\nabla\phi, (\nabla\phi)^3 \dots$ , should be avoid also because of the invariant in the reflection transform. The sign of the parameters  $a_{2n}$  can be decided from the observed pattern *in vivo*.  $(\nabla\phi)^2$  term makes the topologic excitation state, pinwheels in orientation column or vortices in magnetism, and its parameter  $a_2$  should be positive. The parameters  $a_{2n}$  for  $n \geq 2$  should vanish or be positive, otherwise the pattern in the orientation column will emerge with distinct feature. If every parameters  $a_{2n}$  for  $n \geq 1$  are positive, we can take only  $(\nabla\phi)^2$  term in the effective Hamiltonian because the pinwheel formation of the orientation map, the lowest excited state, is decided from this in two-dimensional lattice system. Sometimes the rotation angle  $\chi$  has dependency on position  $\mathbf{r}$ , called the ‘local’ gauge transform, and the effective Hamiltonian should be rewritten as

$$H[\phi] = a_2 \int dr^2 (\nabla\phi - \mathbf{A})^2. \quad (6)$$

The arbitrary vector  $\mathbf{A} = \nabla\chi(\mathbf{r})$ , called the vector potential in magnetism, is very important factor in the visual map formation. The average typical spacing in OP column is decided by  $\Lambda_{OP} = 2\pi/|\mathbf{A}|$ .  $|\mathbf{A}|$  occurs due to the competitive behaviour between neurons or the inhibitory lateral interactions. If  $|\mathbf{A}|$  vanishes, the linear zones in OP column are not emergent. The Hamiltonian in equation (6) is the necessary form of energy function in continuum approximation to develop the two prominent features in OP columnar pattern - pinwheels and linear zones. The mathematical technique which derives the energy function by using only the invariant for the transform in lattice and phase space is a well known method for physicist as *the gauge theory*<sup>35</sup>. We can get also the effective Hamiltonian as a function of the spin components ( $S_x, S_y, S_z$ ) with similar method, which is related the Lagrangian of matter field in  $O(3)$  or  $SU(2)$  symmetry. From the equilibrium condition,  $\delta H/\delta\phi \sim 0$  (or  $\delta H/\delta S_\alpha \sim 0$  for  $\alpha = x, y$  and  $z$ ), we can derive

$$\nabla^2\phi \sim 0 \quad (\text{or } \nabla^2S_\alpha \sim 0), \quad (7)$$

which explains another perpendicular tendency of the iso-orientation contours and the OD bands with the margin of striate cortex. From the normalization constraint, we can obtain again that

$$\nabla S_\alpha \cdot \nabla S_\beta \sim 0 \quad (8)$$

for  $\alpha, \beta \in \{x, y, z\}$ . The gradient vectors  $\nabla S_x|_{S_x=0}$  and  $\nabla S_y|_{S_y=0}$  denote the normal vectors of iso-orientation contours with  $\phi = \frac{\pi}{4}, \frac{3\pi}{4}$  and  $\phi = 0, \frac{\pi}{2}$ , meeting perpendicularly at pinwheels. The normal vectors of the borders of opposite ocular dominance,  $\nabla S_z|_{S_z=0}$ , also have to meet the iso-orientation contours in steep or right angles from (8).

The parameter  $a_2$  and  $\mathbf{A}$  in equation (6) is decided from the detailed map modification rules. For lateral interactions with (3), we can derive that

$$|\mathbf{A}_\mu| = \frac{1}{\sigma_\mu} \sqrt{4 - 1/k_\mu}, \quad (9)$$

or the typical spacing  $\Lambda_\mu = 2\pi/|\mathbf{A}_\mu|$  (see ref. 16), that means (i) the typical spacing  $\Lambda_\mu$  is in proportion to the cooperation range  $\sigma_\mu$  and (ii) the linear zones in OP column or the parallel bands in OD column are emergent when  $k_\mu > 1/4$ . Other models also predict similar results however the bifurcation between homogeneous and inhomogeneous states occurs depending on some other factors.

13. Wolf, F. & Geisel, T. Spontaneous pinwheel annihilation during visual development. *Nature* **395**, 73-78 (1998).
14. Obermayer, K., Blasdel, G. G. & Schulten, K. Statistical-mechanical analysis of self-organization and pattern formation during the development of visual maps. *Phys. Rev. A* **45** 7568-7589 (1992)
15. Goodhill, G. J. & Cimponeriu, A. Analysis of the elastic net model applied to the formation of ocular dominance and orientation columns. *Network*: **11** 153-168 (2000).
16. Cho, M. W. & Kim, S. Understanding visual map formation through vortex dynamics of spin Hamiltonian models. *Phys. Rev. Lett.* (to be published) arXiv:physics/0306047.
17. Löwel, S. Ocular dominance column development: Strabismus changes the spacing of adjacent columns in cat visual cortex. *J. Neurosci.* **14** 7451-7468 (1994).
18. Löwel, S., Schmidt, K. E., Kim, D. S., Wolf, F., Hoffstümmer, F., Singer, W. & Bonhoeffer, T. The layout of orientation and ocular dominance domains in area 17 of strabismic cats. *Eur. J. Neurosci.* **10** 2629-2643 (1998).
19. Löwel S. & Wolf S. Selection of intrinsic horizontal connections in the visual cortex by correlated neuronal activity
20. Sirosh J. & Miikkulainen R. Ocular dominance and pattern lateral connections in a self-organizing model of the primary visual cortex: *Proceeding of the 1994 Neural Information Processing Systems (NIPS) conference*.
21. Albus, K. 14C-Deoxyglucose mapping of orientation subunits in the cat's visual cortical areas. *Exp. Brain Res.* **24** 181-202 (1979).
22. Diao, Y.-C., Jia, W., Swindale, N. V. & Cynader, M. S. Functional organization of the cortical 17/18 border region in the cat. *Exp. Brain Res.* **79** 271-282 (1990).
23. Rao, S. C., Toth, L. J. & Sur, M. Optically imaged maps of orientation preference in primary visual cortex of cats and ferrets. *J. Comp. Neurol.* **387** 358-370 (1997).
24. Bonhoeffer, T., Kim, D.-S., Malonek, D., Shoham, D. & Grinvald, A. Optical imaging of the layout of functional domains in area 17 and across the area 17/18 border in cat visual cortex. *Eur. J. Neurosci.* **7** 1973-1988 (1995).
25. Crowley, J. C. & Katz, L. C. Development of ocular dominance columns in the absence of retinal input *Nature Neurosci.* **2** 1125-30 (1999).
26. Bosking, W. H., Zhang, Y., Schofield, B. R. & Fitzpatrick, D. Orientation selectivity and the arrangement of horizontal connections in tree shrew striate cortex. *J. Neurosci.* **17**, 2112-2127 (1997).
27. Costa, J. E. R. & Costa, B. V. Static and dynamic simulation in the classical two-dimensional anisotropic Heisenberg model. *Phys. Rev. B* **54** 994-1000 (1996).
28. Wysin, W. M. Instability of in-plane vortices in two-dimensional easy-plane ferromagnets *Phys. Rev. B* **49** 8780-8789 (1994).
29. Wysin, W. M. Critical anisotropies of two-dimensional magnetic vortices *Phys. Lett. A* **240** 95-99 (1998).
30. Cho, M. W. & Kim, S. Instability of planar vortices in two-dimensional easy-plane Heisenberg model with distance-dependent interactions. arXiv:cond-mat/0310753.
31. Swindale, N. V. The development of topography in the visual cortex: a review of models. *Network*: **7**, 161-247 (1996).
32. Hoffstümmer, F., Wolf, F., Geisel, T., Löwel, S., & Schmidt, K. Sequential bifurcation of orientation and ocular dominance maps. In ICANN95: *Proceedings of the International Conference on Artificial Neural Networks*, volume I, p. 535-540 (EC2 & Cie, Paris, 1995).

33. Hoffstümer, F., Wolf, F., Geisel, T., Löwel, S., & Schmidt, K. Sequential bifurcation and dynamic rearrangement of columnar patterns during cortical development. In Jim Bower, editor, *Computation and neural systems* (1996).
34. Wolf, F., Pawelzik, K., Scherf, O., Geisel, T. & Löwel, S. How can squint change the spacing of ocular dominance columns? *J. Physiol* **94** 524-537 (2000).
35. Ryder, L. H. *Quantum Field Theory* (Cambridge University Press, 1985).